NJC

Accepted Manuscript

This article can be cited before page numbers have been issued, to do this please use: P. Ray, M. Clément, C. Martini, I. Abdellah, P. Beaunier, J. L. Rodriguez-Lopez, V. Huc, H. Remita and I. Lampre, *New J. Chem.*, 2018, DOI: 10.1039/C8NJ02451K.

ROYAL SOCIETY OF CHEMISTRY

rsc.li/njc

ROYAL SOCIETY OF CHEMISTRY
View Article Online
DOI: 10.1039/C8NJ02451K

Journal Name

ARTICLE

Stabilisation of small mono- and bimetallic gold-silver nanoparticles by calix[8]arene derivatives †

Received 00th January 20xx,
Accepted 00th January 20xx

DOI: 10.1039/x0xx00000x

www.rsc.org/

Priyanka Ray,[a,b] Marie Clément,[a,b] Cyril Martini, [b] Ibrahim Abdellah,[b] Patricia Beaunier,[c] Jose Luis Rodriguez-Lopez,[d] Vincent Huc,[b] Hynd Remita[a] and Isabelle Lampre*[a]

In this paper, we report the synthesis of octa(hydroxy)-octa(mercaptobutoxy)calix[8]arene and its use as stabiliser of nanoparticles (NPs). We show that the reduction of gold and/or silver ions in the presence of this calix[8]arene in ethanolic solutions leads to the formation of very small spherical nanoparticles (NPs), homogeneous in size. Confinement and cooperative effects due to the macrocyclic structure of the calix[8]arenes account for the obtained small sizes and the homogeneity. In the case of the simultaneous reduction of gold and silver ions, STEM-EDX mappings give evidence of the formation of alloyed Au-Ag NPs stabilised by calix[8]arenes. The surface accessibility and potential catalytic applications of the NPs are tested using the reduction of 4-nitrothiophenol by $NaBH_4$ as a model reaction..

Introduction

Metal nanoparticles (NPs) are increasingly attracting attention due to their unique properties[1-5] and potential applications[6] in catalysis,[7-10] optical[11, 12] and magnetic devices,[13, 14] imaging, sensors[15] and medecine.[16, 17] The properties of metal NPs which differ from the bulk arise from large surface to volume ratio, surface energy and spatial confinement and depend on the size and shape of the NPs. For example, for noble metal NPs, the decrease in size below the electron mean free path induces coherent oscillations of the free electrons and leads to intense absorption band in the UV-visible range called the surface plasmon resonance (SPR). In the case of silver (Ag) and gold (Au) NPs, this SPR band is situated around 400 nm and 500 nm, respectively.[18-20] Noble metal nanostructures may also possess surface-enhanced Raman scattering (SERS) activity.[21, 22] In addition to these remarkable optical properties, Ag and Au NPs display catalytic activities[23, 24] and raise great interest for biomedical applications.[25-28]

In order to avoid their coalescence and aggregation, metal clusters and small metal NPs have to be stabilised by polymers, ligands or immobilised on supports. Lately, macrocycles such as cyclodextrin,[29, 30] cucurbituril[31, 32] or calixarene,[33, 34] have emerged as interesting ligands. In particular, calixarenes appear very attractive due of their conformational behaviour, their chemical versatility and their host-guest properties.[35, 36] On the one hand, the stabilisation of NPs by ligands possessing multiple anchoring groups such as calixarenes strongly improves the grafting stability of the ligand shell because of the cooperative binding of these groups.[29, 33] On the other hand, weakly bonded arms can be used without compromising on the stability of the NPs. The lability of each individual bond between the anchoring group and the nanoparticle surface may enhance the reactivity and stability of these nanoobjects in catalysis. In fact, calixarene-bound metal NPs demonstrate high levels of surface accessibility,[37-39] which is critical for catalysis.[40] The presence of such organic ligands can also increase the robustness of metal NPs against sintering which is an acute problem in catalysis. Several examples of calixarene-stabilised nanoparticles have already been reported.[33, 34, 37-44]

In this article we demonstrate that the octa(hydroxy)-octa(mercaptobutoxy) calix[8]arene **5** (Chart 1a) can stabilise very small metallic NPs produced by γ-radiolysis in ethanol. Numerous methods are used to prepare metallic NPs. Among the reduction methods (chemical, radiolytical, photochemical, electrochemical, sonochemical…), radiolysis is a powerful tool

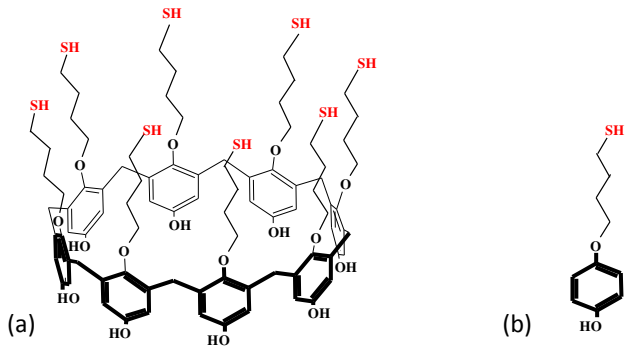

Chart 1 Structure of **(a)** the *p*-octa(hydroxy)-octa(mercaptobutoxy) calix[8]arene **5** and **(b)** the corresponding 4-(4-mercaptobutoxy)phenol monomer

[a] *Laboratoire de Chimie Physique, Univ Paris-Sud UMR 8000 CNRS, Université Paris-Saclay, 91405 Orsay cedex, France. E-mail:isabelle.lampre@u-psud.fr*
[b] *Institut de Chimie Moléculaire et des Matériaux d'Orsay, Univ Paris-Sud UMR 8182 CNRS, Université Paris-Saclay, 91405 Orsay cedex, France*
[c] *Sorbonne Université, CNRS, Laboratoire de Réactivité de Surface, UMR 7197, F-75005 Paris cedex 05 (France)*
[d] *Advanced Materials Departement, IPYCIT, A.C., 78216 San Luis Potosi, Mexico*

† Electronic Supplementary Information (ESI) available: experimental details and characterisations for the synthesis of calix[8]arene 5 and 4,4'-mercaptobutoxyphenol; TEM, XPS and EDX analysis of NPs are provided. See DOI: 10.1039/x0xx00000x

View Article Online
DOI: 10.1039/C8NJ02451K

to synthesise nanoparticles of controlled size and shape in solutions and in heterogeneous media.[45-48] The reducing species (solvated electron and radicals) are generated from the solvent by ionising radiation.[49-51] Hence, no chemical reactants are needed to reduce the metal, what limits the contamination of the growth solution.

Here, we present the synthesis of the *p*-octa(hydroxy)-octa(mercaptobutoxy)calix[8]arene and its use for the radiolytic synthesis of mono- and bi-metallic Au-Ag NPs. The *p*-octa(hydroxy)-octa(mercaptobutoxy)calix[8]arene **5** used as stabiliser is functionalised on the lower rim by thiol groups allowing the anchoring on metallic surfaces and on the upper rim by hydroxyl groups which ensure a dispersion in polar and protic solvents such as ethanol and may be used for post-derivatisation of the formed nanoobjects. We show that calix[8]arene **5** is able to stabilise small NPs, homogeneous in size and with an alloyed structure in the case of the Au-Ag system. Various silver precursor salts and different ratios between metallic ions and calix[8]arenes were tested in order to study the influence of the counter ion and the salt concentration on the obtained NPs. The stabilising power of the calix[8]arene is also compared to its monomer, the 4-(4-mercaptobutoxy)phenol (Chart 1b). The reduction of 4-nitrothiophenol (4-NTP) is used as a model reaction[52, 53] to test the catalytic activity of the NPs.

Experimental

Materials

Most solvents and all reagents were obtained from commercial supplies and used without purification. Silver perchlorate monohydrate ($AgClO_4 \cdot H_2O$, purity ≥99.999%), silver hexafluoro phosphate ($AgPF_6$, purity ≥98%) silver tetrafluoroborate ($AgBF_4$, purity ≥98%), silver trifluoromethanesulfonate ($AgCF_3SO_3$ noted AgOTf, purity ≥99%), tetrachloroauric acid trihydrate ($HAuCl_4$, $3H_2O$, purity ≥99.99%) and 4-nitrothiophenol (4-NTP, purity ≥80%) were purchased from Sigma-Aldrich. Absolute ethanol (AnalaR Normapur, >99.8%) was obtained from VWR Prolabo.

Instrumentation

The irradiation source was a ^{60}Co γ-facility; the used dose rates were 1.8 and 3.7 kGy h^{-1}. The dose in ethanol was determined from the measurement in water by the Fricke dosimeter method and by taking into account the relative electronic density factor (which is 0.8 for ethanol).

^1H and ^{13}C NMR spectra were recorded on Brüker Avance spectrometers at 298 K. Electrospray Ionisation Mass Spectrometry (ESI-MS) data were collected using a Brüker 2009 spectrometer.

UV-visible absorption spectra were taken with a single beam Hewlett-Packard 8453 spectrophotometer with a 2 nm resolution or with a two beams Cary 60 spectrometer. Catalytic tests were recorded by an immersion optic probe Hellma with argon flow and equipped with two optic fibers linked to the spectrophotometer. The scanning rate used to record the spectra with Cary WinUv (« scan » or « scanning kinetics » modes) was 2016 nm.min^{-1}.

The emission measurements were performed with a Horiba Jobin Yvon Fluoromax 4P. Due to the high absorbance of the prepared samples, dilutions were performed in order to reduce the maximum absorbance below 0.1 in the conventional 1 cm × 1 cm quartz cell used; the emission spectra were then registered in the right angle configuration. Excitation and emission bandwidths were set to 10 and 1 nm, respectively.

Fourier transform infrared (FTIR) spectra of samples prepared as KBr pellets were obtained with a Perkin-Elmer Spectrum 100 at a resolution of 4 cm^{-1}. All measurements were carried out at room temperature.

X-ray photoelectron spectroscopy (XPS) was performed on a PHI 5000 VersaProbe II (Physical Electronics) equipped with a monochromatic Aluminum source (Al, K_α = 1486.6 eV, beam size: 100 µm; X-ray voltage: 15 kV; power: 25 W). Samples were introduced, without prior surface cleaning, on copper tape. Charge neutralization was performed by irradiation of the surface with low energy electrons (5 eV maximum).The spectra were recorded with a 117.3 eV pass energy for the survey acquisition and a 23.5 eV pass energy for narrow scans.

Transmission electron microscopy (TEM) images were recorded with either a JEOL JEM 100CX or a FEI TECNAI F30 transmission electron microscope operating at an accelerating voltage of 100 kV and 300 kV, respectively. For high resolution electron microscopy (HRTEM) images, a JEOL JEM 2010 equipped with a LaB_6 filament and operating at 200 kV was used. The images were collected with a 4008 X 2672 pixels CCD camera (Gatan Orius SC1000). Samples for TEM analysis were prepared by drops of irradiated solutions deposited and dried on carbon-coated copper grids for TEM observations.

Scanning transmission electron microscopy (STEM) experiments were carried out on a FEI Titan G2 transmission electron microscope operating at 200 kV and equipped with a detector for high angle annular dark field (HAADF) imaging and a detector for energy dispersive X-ray (EDX) mapping.

Radiolytic synthesis of NPs

Preparation of samples for radiolytic reduction. To synthesise the stabilised metallic nanoparticles, the metallic salts and the calix[8]arene **5** (or 4-(4-mercaptobutoxy)phenol) were first dissolved separately in ethanol to obtain stock solutions. Second, adapted volumes of the stock solutions and ethanol were mixed to obtain the desired concentrations. Then, the solutions containing metallic ions and calix[8]arene **5** (or monomer) were deaerated prior to irradiation by bubbling with nitrogen (N_2, from Air Liquide, U grade, purity 99.999%) and kept under N_2 atmosphere during irradiation. The prepared ethanolic solutions containing different concentrations of metallic salts (ranging from 5×10^{-4} M to 10^{-3} M) and 5×10^{-5} M calix[8]arene **5** (or 4×10^{-4} M monomer) were subjected to γ-irradiation till total reduction of metallic ions.

Radiolytic reduction and NPs formation. Ethanolic solutions containing metallic salts and calix[8]arene (or monomer) were

View Article Online
DOI: 10.1039/C8NJ02454K

exposed to γ-rays. The primary effects of irradiation by high energy radiation are the ionization and excitation of the solvent molecules, ethanol:

$$C_2H_5OH \xrightarrow{\gamma} (C_2H_5OH)^{\bullet+} + e^- + C_2H_5OH^* \quad (1)$$

This primary step is followed by the dissociation of excited states, the solvation of the electron and a reaction of the parent cation with another ethanol molecule yielding the radical and the protonated form of the ethanol molecule: [50, 54-58]

$$C_2H_5OH^* \rightarrow CH_3C^{\bullet}HOH + H^{\bullet} \quad (2)$$

$$e^- \rightarrow e^-_{solv} \quad (3)$$

$$(C_2H_5OH)^{\bullet+} + C_2H_5OH \rightarrow CH_3C^{\bullet}HOH + C_2H_5OH_2^+ \quad (4)$$

The formed solvated electrons reduce the metallic ions M^{q+} homogeneously in the medium till zero-valent metal atoms. Then, the atoms dimerize when they encounter another atom or ion and further coalescence/association processes lead to the formation of clusters and NPs.[45, 48]

The alcohol radicals are known to have reducing properties and take part in metallic ions reduction. Their redox potential determined in water ($E°(CH_3CHO,H^+ / CH_3C^{\bullet}HOH) = -1.25\ V_{NHE}$)[59] is more negative than that of Au^{III}/Au^{II} [60] but more positive than that of the couple Ag^+/Ag (in the range -1.8 down to -2.6 V_{NHE} depending on the ligand).[61-65] That would exclude a direct reduction of Ag^+, but not of Au^{III}. However, as the redox potential of metallic clusters M_n^{x+} increases with the nuclearity, reduction of metallic ions adsorbed on clusters becomes thermodynamically possible.[66, 67] Moreover, transient complexation between metallic ions and alcohol radicals before reduction has also been reported for Ag^+ [68] and for Au^{III} and Au^I.[69] Thus, the radicals can contribute to the reduction of metallic ions in the ethanolic solution. In the case of solutions containing two ionic metallic precursors M^{q+} and M'^{z+}, solvated electrons and radicals reduce ions with statistical probabilities and mixed coalescence/association phenomena follow. But, electron transfers between the different valencies of both metals may also occur, what can play a role on the final structure of the formed bimetallic NPs (core-shell or alloy).[67, 70]

Results and discussion

p-Octa(hydroxy)-octa(mercaptobutoxy)calix[8]arene 5

The synthetic procedure towards octa(hydroxy)-octa(mercaptobutoxy)calix[8]arene **5**, used in this work, is described in Scheme 1. Calix[8]arene **5** is obtained from the benzyloxyphenol in five main steps with an overall yield of 37%. Briefly, the benzyloxycalix[8]arene **1**, is first synthesized from benzyloxyphenol according to the previously reported procedure.[41, 71] Then, compound **2** is prepared by nucleophilic substitution between calix[8]arene **1** and 1-bromo-4-chlorobutane after deprotonation of the OH group of calix{8}arene **1** by NaH. The next step consists in the debenzylation of the upper rim using $Pd(OH)_2$ in the presence of cyclohexene. In the fourth step, a nucleophilic attack occurs

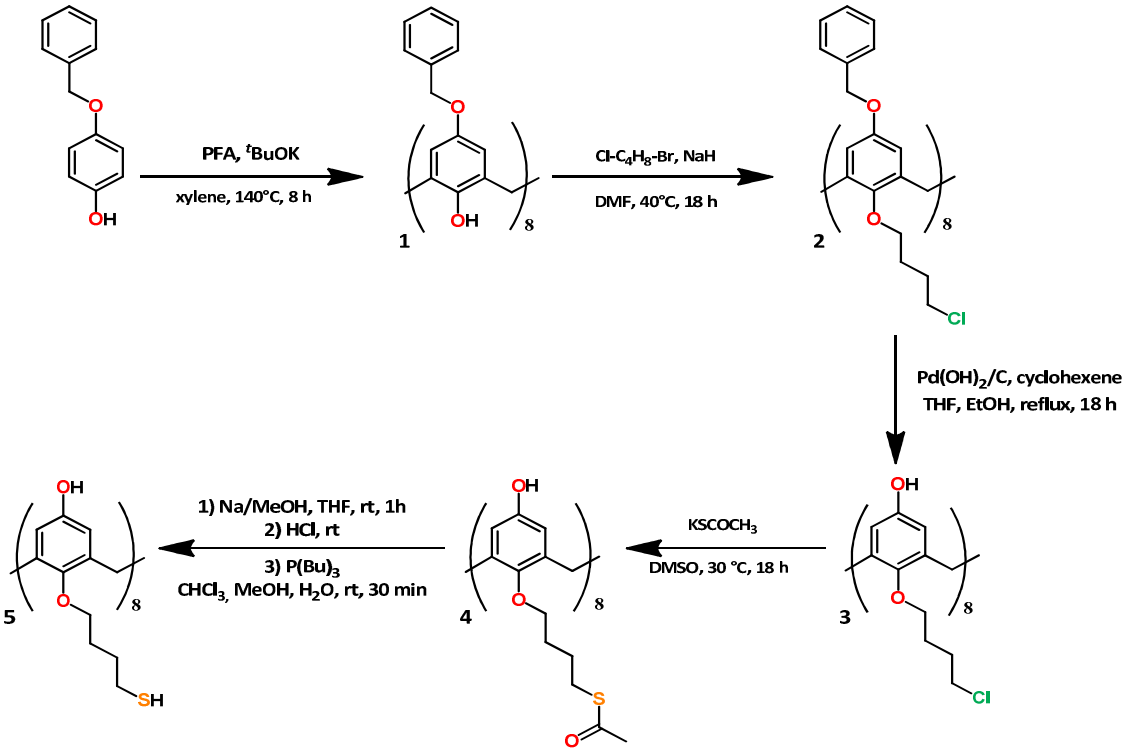

Scheme 1: Synthetic route towards the octa(hydroxy)-octa(mercaptobutoxy) calix[8]arene **5**

View Article Online
DOI: 10.1039/C8NJ04451K

and the chlorine atom is substituted by a thioacetate group. Finally, hydrolysis performed with sodium methanoate leads to the desired calix[8]arene **5**. Experimental details and characterisation (NMR, IR, MS) are provided in ESI†. It is worth noticing that the ^{1}H NMR spectrum of calix[8]arene **5** (Fig. S1, ESI†) presents well-resolved symmetrical and narrow signals due to the symmetry and high flexibility of the molecule in solution. This validates both the formation and purity of the compound. Indeed, one advantage of calix[8]arenes compared to calix[4]arenes is their higher conformational flexibility, even with bulky substituents on the lower rim, in line with an easier purification. Calix[4]arenes tend to lock in various conformers as the hydroxyl groups on the lower rim are substituted, and conformers purification is often difficult.

The synthesized calix[8]arene **5** is soluble in ethanol due to the presence of the hydroxyl groups. The absorption spectrum of the obtained solution presents a band in the UV spectral range with a maximum absorption wavelength λ_{max} at 288 nm and an extinction coefficient ε_{max} of 24650 ± 2400 L mol^{-1}cm^{-1} (Fig. 1a). When excited in its absorption band, the calix[8]arene **5** exhibits a fluorescent spectrum between 300 and 400 nm with a maximum at 327 nm (Fig. 1 inset). The large Stokes shift (4140 cm^{-1}) may be related to solvent effects and conformational changes in the excited state due to the high flexibility of the molecule in solution.

Silver nanoparticles

Ag NPs were first synthesised as various silver salts with different counter ions are readily available and several parameters were studied. Initially, the same ratio between calix[8]arene and metallic atoms as those previously reported,{Huc, 2008 #17} i.e. 10 eq. Ag^+ and 1 eq. calix[8]arene **5** were used. Then, the amount of Ag^+ ions was increased to investigate the influence of this ratio on the size of the synthesised NPs. Different precursor salts were also taken to study the influence of the counter ion. The efficiency of the stabilisation by the calixarene is compared to its monomeric counterpart.

Synthesis from $AgClO_4$ salt with Ag^+/calix ratio of 10. An ethanolic solution containing 5×10^{-4} M $AgClO_4$ and 5×10^{-5} M calix[8]arene **5** was prepared. Just after the mixing of the $AgClO_4$ solution with the calix[8]arene **5** solution, in addition to the calix[8]arene **5** peak, the absorption spectrum presents a light scattering pattern in the UV spectral domain indicating an aggregation phenomenon. However, after overnight stirring, this pattern vanishes and the initial peak of calix[8]arene **5** at 288 nm decreases in intensity and broadens while a new band at 237 nm appears (Fig. 1c), suggesting a complexation of calixarenes with silver ions. Calixarene complexes with silver ions have already been reported for calixarenes containing sulphur atoms.[72] Interactions between calixarenes and Ag^+ ions are also corroborated by fluorescence measurements. After addition of $AgClO_4$ to the calixarene solution, the fluorescence emission vanishes (Fig. 1 inset). The quenching of the fluorescence indicates a change in the relaxation pathways of excited calixarenes due to interactions with silver ions, in particular spin-orbit coupling favouring intersystem crossing, and also probably modifications of conformations. It is to note that the fluorescence properties of calixarenes have already been investigated to get information on aggregation, formation of complexes or metal cation interactions for potential applications in metal cation sensing.[73-76]

After γ-irradiation of the ethanolic solution containing 5×10^{-4} M $AgClO_4$ and 5×10^{-5} M calix[8]arene **5**, the absorption spectrum of the solution (Fig. 1d) is close to that of the non-irradiated solution (Fig. 1c): the two absorption bands at 237 and 288 nm are still present and their intensities are slightly modified. No surface plasmon resonance (SPR) band of silver

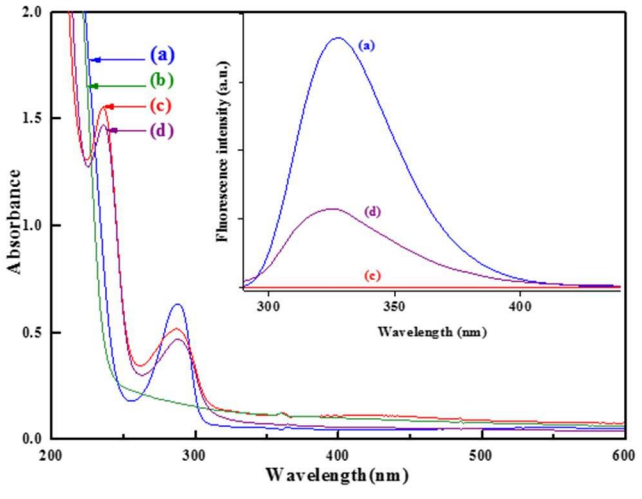

Fig. 1 UV-visible absorption spectra of ethanolic solutions containing **(a)** 5×10^{-5} M calix[8]arene 5, **(b)** 5×10^{-4} M $AgClO_4$, **(c)** 5×10^{-5} M calix[8]arene **5** and 5×10^{-4} M $AgClO_4$ after overnight stirring prior to irradiation and **(d)** 5×10^{-5} M calix[8]arene **5** and 5×10^{-4} M $AgClO_4$ after overnight stirring and irradiation till total reduction (dose 720 Gy) ; optical path = 5 mm; inset: fluorescence spectra of the solutions after dilution to reach an absorbance below 0.1 at the excitation wavelength λ_{exc} = 280 nm in a 1 cm cuvette.

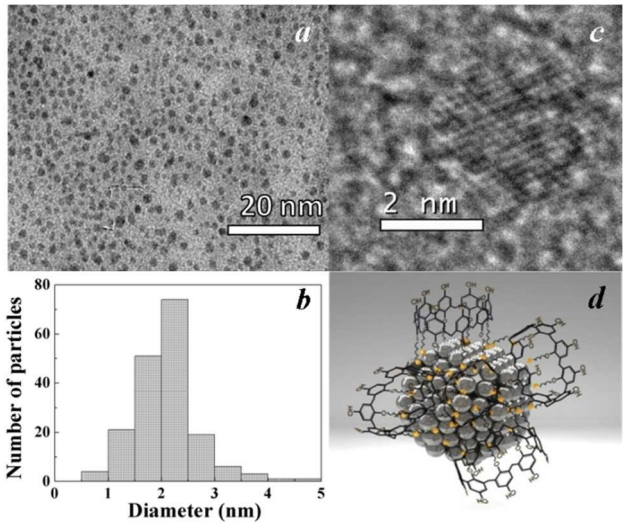

Fig. 2 (a) TEM image and **(b)** size distribution of silver nanoparticles stabilised by calix[8]arenes **5** obtained by total radiolytic reduction of ethanolic solution containing 5×10^{-4} M $AgClO_4$ and 5×10^{-5} M calix[8]arene **5** (dose 720 Gy); **(c)** HR TEM of one NP; **(d)** Scheme illustrating a small silver nanoparticle stabilised by calix[8]arenes **5**.

NPs around 400 nm is observed, suggesting the formation of very small silver nanoparticles. When excited at 280 nm, the irradiated solution presents fluorescence properties, but the emission intensity is lower compared to that obtained for the free calixarene. Moreover, the emission spectrum differs slightly from the fluorescence spectrum of the free calix[8]arene: the band presents a small hypsochromic shift (λ_{max} = 324 nm) and is broader with an emission tail in the red side (around 385 nm). Consequently, the observed spectrum cannot be attributed only to free calix[8]arenes **5** but also to the calix[8]arenes **5** linked to silver NPs.

Fig. 2a and b illustrate the typical TEM images and size distribution of the samples obtained after γ-irradiation to total reduction of a solution containing 5×10^{-4} M $AgClO_4$ and 5×10^{-5} M calix[8]arene **5**. The observations reveal the formation of small NPs very homogeneous in size with a mean diameter of 2 nm. High-resolution TEM images (Fig. 2c) indicate that the produced NPs are crystalline with the typical face-centred cubic structure of bulk silver. The obtained silver NPs are small and much more monodisperse compared to other calixarene stabilised Ag NPs reported in the literature.[42-44] A scheme depicting a silver nanoparticle stabilised by calix[8]arenes **5** is shown in Fig. 2d.

The presence of calix[8]arenes on Ag NPs was evidenced by FTIR analysis. Isolation of the Ag NPs was performed by centrifugation and intensive and successive washing of the nanoparticles in DCM, followed by pentane. The obtained FTIR spectrum of the Ag NPs stabilised by calix[8]arenes **5** presents the characteristic of the free calix[8]arenes **5** (Fig. 3), indicating that no alteration of the chemical structure of the ligands occurs during the γ-irradiation. However, the disappearance of the S-H stretching at 2561 cm^{-1} shows that calix[8]arenes are adsorbed on nanoparticles via S-Ag bond and very few mercaptobutyl chains remain ungrafted.

It is worth noticing that if the Ag^+/calix ratio is kept constant and equal to 10 but the concentrations of both metallic salt and calix[8]arene are multiplied by 10, after total reduction, the formed Ag NPs keep similar size (around 2 nm) and size distribution.

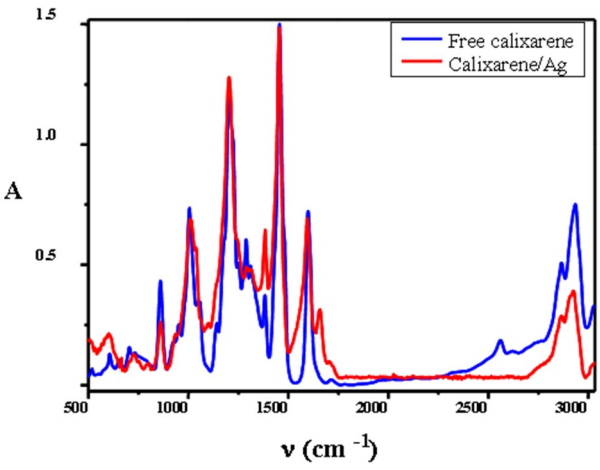

Fig. 3 FTIR spectra (normalized at 1.5).of calix[8]arenes alone (blue) and grafted on silver nanoparticles (red).

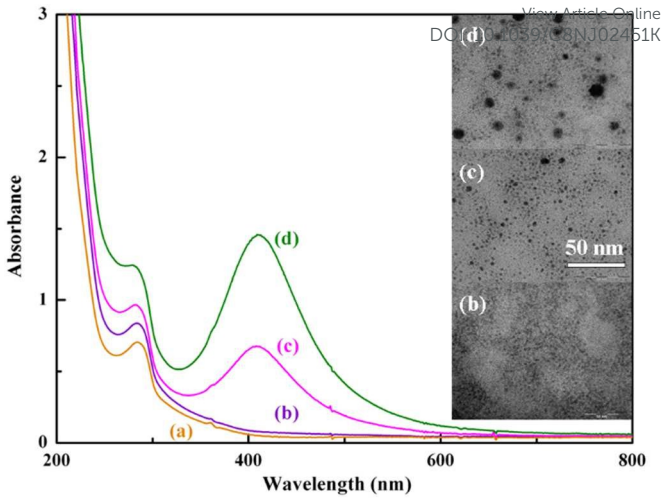

Fig. 4 UV-visible absorption spectra of ethanolic solutions containing 5×10^{-5} M calix[8]arene and various concentrations of $AgClO_4$: **(a)** 5×10^{-4} M just after mixing prior to irradiation, **(b)** 5×10^{-4} M after irradiation till total reduction §, **(c)** 7.5×10^{-4} M after irradiation till total reduction, **(d)** 1×10^{-3} M after irradiation till total reduction (optical path = 5 mm); inset: TEM images of the obtained silver nanoparticles (the scale is the same for the three micrographs).

Increase of the ratio Ag^+/calix. Given the previous size distribution obtained and considering a cuboctahedral close packed arrangement of successive shells of metal atoms, these NPs could correspond mainly to 3-shells nanocrystals composed of 147 atoms and having a diameter of 2 nm.[77, 78] Assuming that at most each surface atom (92 per NP) is linked to sulphur and all the sulphur atoms of one calixarene are in interactions with the NP, up to 11 calix[8]arenes could be grafted on a Ag NP. So, at least 25% of the present calix[8]arene should remain free in solution, and available to stabilise more NPs. So, experiments were performed with solutions containing the same concentration of calix[8]arene **5** (5×10^{-5} M) but higher concentrations of $AgClO_4$ (7.5×10^{-4} and 1×10^{-3} M).

After γ-irradiation, the UV-visible absorption spectra of the totally-reduced solutions present the characteristic SPR band of silver NPs around 410 nm and TEM images reveal the presence of large NPs (Fig. 4). The average size of the formed silver NPs is 3.5 nm for 7.5×10^{-4} M $AgClO_4$ and around 6 nm for 1×10^{-3} M but with a very broad distribution in sizes (Fig. S2, ESI†). The size and the size distribution of the produced NPs increase with the concentration of silver ions suggesting that there are not enough calix[8]arene molecules available to stabilise small NPs. This indicates that the stabilisation of small NPs requires a good coating of the surface and so an adequate metal to calix[8]arene ratio.

Effect of the counter ion. The previous Ag NP were synthesised from the perchlorate salt. In order to study the influence of the counter ion, three other salts were tested: $AgPF_6$, $AgBF_4$ and AgOTf. Ethanolic solutions containing 5×10^{-5} M calix[8]arene **5** and 5×10^{-4} M Ag^+ salt (ratio Ag/calix = 10) were prepared and

View Article Online DOI: 10.1039/C8NJ02451K

irradiated till total reduction. The TEM images and the size distribution of the obtained Ag NPs are given in Fig. S3, ESI†. An effect of the counter ion is detected as the average size of the NPs increases from 1.5 to 5.5 nm in the order $AgPF_6$ < $AgClO_4$ < AgOTf < $AgBF_4$, but in all cases the NPs remain small and homogeneous in size. The effect observed on the size of the NPs cannot be related to the shape and size of the counter ion. Indeed, their volume have been reported to be (in Å^3): 53.4, 54.4, 73.0 and 86.9 for BF_4^-, ClO_4^-, PF_6^- and $CF_3SO_3^-$, respectively.[79] So, $AgBF_4$ and $AgClO_4$ should have given NPs with similar sizes, smaller than those obtained with $AgPF_6$ and AgOTf, what is not the case. The salt effect might be explained by the coordinating power of the counter ion and the strength of the ionic interactions leading to various proportions of free ions, ion pairs and ionic aggregates and consequently to different numbers of Ag^+ ions complexed to calix[8]arenes **5** in ethanol. For instance, in their study on the ionic interactions in π-complexes of poly(hexamethylene vinylene), PHMV, with silver salts, Kim et al. reported that the coordination number of silver ion for C=C of PHMV was in the order $AgBF_4$ > $AgClO_4$ > AgOTf.[80] In our case, a higher number of Ag^+ complexed to one calixarene would favour the first associations between atom and non-reduced ions as no diffusion is required, what would reduce the number of initial clusters. A reduced number of seeds would lead to a decrease in the number of NPs and an increase in their size.

Stabilising efficiency of calixarenes. Experiments were also conducted in the presence of the monomeric analogue, 4-(4-mercaptobutoxy)phenol, of which synthesis is described in ESI†. Ethanolic solutions containing 5×10^{-4} M $AgClO_4$ and 4×10^{-4} M 4-(4-mercaptobutoxy)phenol were prepared to keep the same concentration of sulphur atom as with calix[8]arene **5**. After γ-irradiation till total reduction, the UV-visible absorption spectra of the solutions exhibit the characteristic SPR band of silver NPs with a maximum at 420 nm (Fig. 5) attesting the presence of large Ag NPs. TEM observations confirm the formation of very inhomogeneous in size and shape Ag NPs, with a mean diameter of 13 nm (Fig. 5 inset). These results show that the stabilisation of small Ag NPs is dramatically dependent on the confinement and cooperative effect ensured by the calixarene geometry and its eight anchoring arms.

Gold and bimetallic gold-silver nanoparticles

There is a great interest in bimetallic NPs due to synergistic effects of the two metals leading to different optical, electronic and catalytic properties with respect to their monometallic counterparts and also modifications of chemoselectivity and reactivity in catalysis.[81, 82] So, the ability for calix[8]arene **5** to stabilise bimetallic NPs generated by γ-irradiation of mixed solutions of ionic precursors was also tested. Because of the applications Au-Ag bimetallic NPs in numerous domains. [83-86], we have also investigated the gold-silver system.

Gold nanoparticles. An ethanolic solution containing 5×10^{-4} M $HAuCl_4$ and 5×10^{-5} M calix[8]arene **5** was prepared and γ-irradiated till total reduction. Fig. 6 presents the absorption spectra of the mixed solution before and after γ-irradiation as well as the absorption spectrum of each compound alone in solution. The absorption spectrum of the mixed solution shows two absorption bands at 291 and 321 nm, corresponding to calix[8]arene **5** and $HAuCl_4$, respectively, since, in contrast to $AgClO_4$, the ethanolic solution of $HAuCl_4$ presents an absorption band at 321 nm. However, the spectrum of the mixed solution differs from the sum of the two spectra of the compounds indicating, as in the case of $AgClO_4$, interactions and complexation phenomena between calix[8]arenes **5** and Au^{III} ions. After γ-irradiation, the absorption band associated to $HAuCl_4$ is no longer present, but a new broad band has appeared around 530 nm, corresponding to the characteristic surface plasmon resonance band of Au NPs. This indicates the

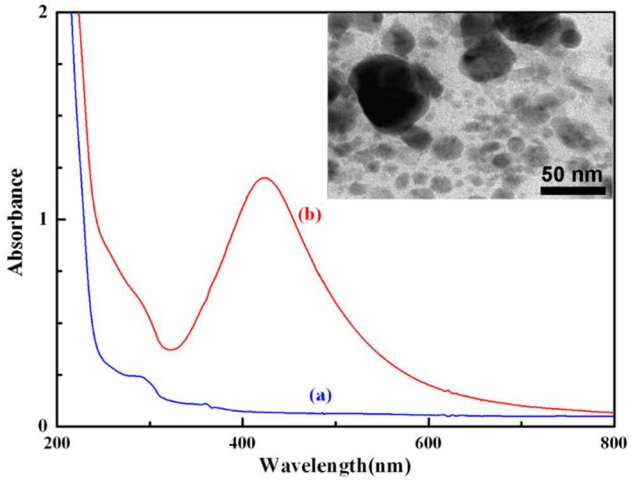

Fig. 5 UV-visible absorption spectra of ethanolic solutions containing 4×10^{-4} M 4-(4-mercaptobutoxy)phenol and 5×10^{-4} M $AgClO_4$ **(a)** prior to irradiation and **(b)** after irradiation till total reduction (dose 720 Gy) ; optical path = 5 mm; inset: TEM image of the obtained silver nanoparticles

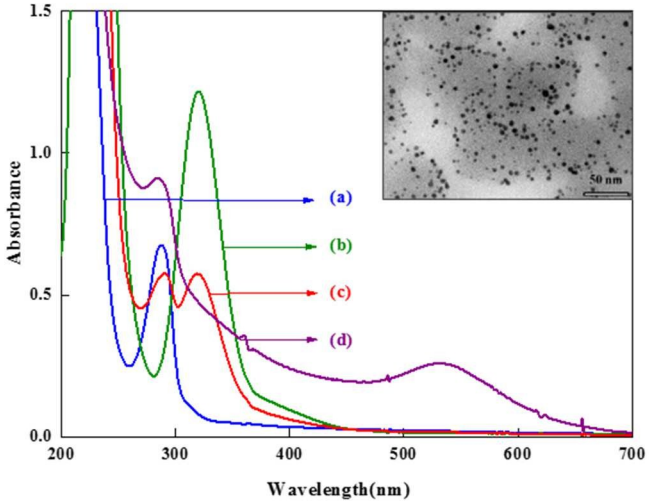

Fig. 6 .UV-visible absorption spectra of ethanolic solutions containing **(a)** 5×10^{-5} M calix[8]arene **5**, **(b)** 5×10^{-4} M $HAuCl_4$, **(c)** 5×10^{-5} M calix[8]arene **5** and 5×10^{-4} M $HAuCl_4$ prior to irradiation and **(d)** 5×10^{-5} M calix[8]arene **5** and 5×10^{-4} M $AgClO_4$ after irradiation till total reduction (dose 2160 Gy) ; optical path = 5 mm), inset: TEM image of the formed Au NPs

View Article Online
DOI: 10.1039/C8NJ02451K

formation of NPs with sizes higher than 5 nm, what is corroborated by TEM analysis (Fig. 6, inset). The size distribution extends from 1.5 to 8.5 nm with an average value of 4.5 nm (Fig. S4, ESI†). The size distribution of the Au NPs is broader than that obtained for Ag NPs with the same metal/calix ratio (10). The ionic precursor used for gold NPs being $HAuCl_4$, the total reduction of the trivalent Au^{III} requires a dose three times higher than that necessary for the reduction of Ag^{I} and occurs via a multistep process involving disproportionation reactions. That induces changes in ionic interactions, dissociation and complexation phenomena, and may affect association and coalescence steps.

Bimetallic Gold-Silver nanoparticles. The synthesis of bimetallic Au-Ag NPs were carried out using $HAuCl_4$ salt and different silver salts but the Au/Ag and metal/calix ratios were kept constant and equal to 1 and 10, respectively. The absorption spectrum of the ethanolic solution containing gold, silver and calix[8]arene before irradiation shows the characteristic absorption bands of calix[8] arene **5** and Au^{III}. After irradiation, the band of Au^{III} has vanished but no characteristic surface plasmon resonance band for Ag or Au NPs is present. TEM images (Fig. 7) reveal the formation of very small spherical NPs with an average size of 3.5 nm. Whatever the silver salt used ($AgPF_6$, $AgClO_4$, AgOTf), similar results are obtained (Fig. S5, ESI†), only a very small effect is observed on the size of the NPs, but weaker than that observed in the case of monometallic silver NPs. The HR-TEM images reveal that the NPs are well crystallised as the crystallographic planes can be observed (Fig. 7) but as gold and silver have very similar lattice parameters, 4.08 and 4.09 Å, respectively, it is difficult to conclude on the structure of the bimetallic NPs. However, from XPS characterisation, it can be inferred that the NPs possess a bimetallic structure. The wide-scan spectrum (Fig. S6, ESI†) shows the presence of silver, gold, sulphur and oxygen. Fig. 8 presents the XPS spectra recorded for the S2p, Ag3d and Au4f regions. The signal for S2p appears as a broad asymmetric peak at 163.7 eV (Fig. 8 top). The fitting procedure requires two spin-orbit doublets ($S2p_{3/2}$ and $S2p_{1/2}$ contributions with $\Delta E \cong 1.2$ eV). The first doublet with the main $S2p_{3/2}$ contribution centred at 162.6 eV can be assigned to sulphur bound to metal (Ag or Au) atom (chemisorption), while the second doublet ($S2p_{3/2}$ peak at 163.7 eV) can be related to unbound or wealkly bound (physisorption) sulphur on the NP surfaces, most likely to R-SH or S-S states.[87-91] The signal of Ag3d corresponds to a well-separated spin-orbit doublet ($\Delta E = 6.0$ eV) with the contributions of $Ag3d_{5/2}$ and $Ag3d_{3/2}$ peaking at 368.4 and 374.4 eV, respectively (Fig. 8 middle) and is attributed to Ag^0. However, the signal to noise ratio is too poor to exclude the presence of a small contribution of more oxidised silver as referred positions for both Ag^0 and Ag^I are very close.[88, 91-93] The present chemical shift of 0.2 eV with respect to reported Ag metal (368.2 eV) could be attributed to an oxidised environment and the peak could also be considered as a mixture of Ag metal and Ag_2S (reported binding energy 368.1 eV) states. The signal of Au4f appears also as a doublet with $Au4f_{7/2}$ and $Au4f_{5/2}$ peaks at 85.0 and 88.4 eV, respectively (Fig. 8 bottom). But, the fitting procedure allows identifying the presence of two doublets. The first $Au4f_{7/2}$ component centred at 84.6 eV is attributed to metallic Au atoms, whereas the second component located at 85.3 eV corresponds to positively charged atoms and is associated to surface gold atoms that are chemically bonded to the calixarene sulphur.[87, 91, 94, 95] Therefore, the XPS characterisations attest the formation of Au-

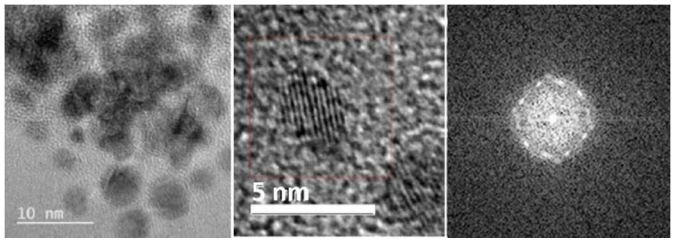

Fig. 7 TEM (left), HR-TEM (middle) images and corresponding FFT projection of Au-Ag NPs stabilised by calix[8]arenes **5** synthesised by γ-irradiation till total reduction (dose 1440 Gy) of a solution containing 5×10^{-5} M calix[8]arene **5**, 2.5×10^{-4} M $AgClO_4$ and 2.5×10^{-4} M $HAuCl_4$

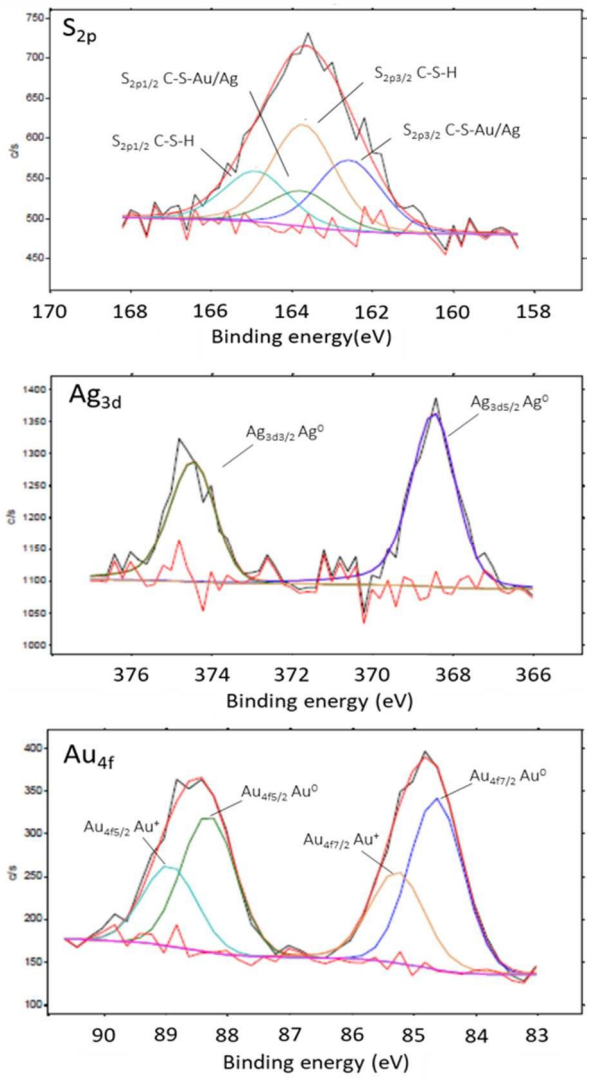

Fig.8: XPS spectra of S2p, Ag3d and Au4f core levels of the produced bimetallic Au-Ag NPs stabilised by calix[8]arenes **5**.

View Article Online
DOI: 10.1039/C5NJ01451K

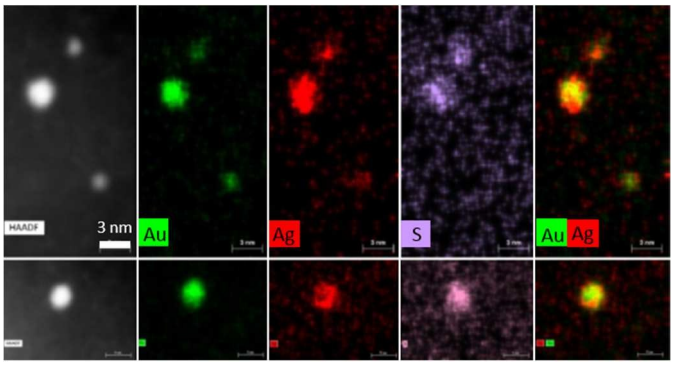

Fig. 9 (left) HAADF-STEM images of the produced bimetallic Au-Ag NPs stabilised by calix[8]arenes **5** and (middle) elemental EDX maps for Au (green), Ag (red) and S (violet) and (right) the superposition of the Au and Ag maps.

Ag NPs with calix[8]arene **5** grafted on the surface. To get more information on the structure of the NPs, HAADF and EDX STEM images were recorded (Fig. 9). It is noteworthy that, in addition to the expected small bimetallic NPs (with sizes around 3 nm), the HAADF-EDX-STEM images reveal the presence of smaller clusters with sizes below 1 nm, not visible in conventional TEM. The elemental maps for gold, silver and sulphur confirm the presence of both metallic atoms in the NPs as well as the presence of sulphur, i.e. of calix[8]arene **5** stabilising the NPs. The superposition of Ag and Au maps indicates the formation of alloyed Au-Ag NPs but with a non-homogeneous distribution of the metals: in the NPs, domains richer in gold and others richer in silver are observed. This non-homogeneous structure can be the result of aggregation of very small clusters. Moreover, the elemental quantifications tends to indicate various ratios of gold and silver in the analysed NPs (fig. S7, and Table S1, ESI†), *i.e.* a non-constant composition of the bimetallic NPs. Such variations may be related to various initial complexations between Au^{III}, Ag^{I} and calixarenes inducing different nucleation seeds which would be followed by non-equivalent coalescence/association processes. A better knowledge (and control) of the initial species present in solution seems necessary to improve the homogeneity of the alloyed Au-Ag NPs formed by radiolysis. So, works are in progress to get a better knowledge on this step, in particular with the synthesis of calixarene-metal complexes with given number of metallic centres.

Catalytic properties

In order to test possible applications of the calix[8]arenes-stabilised NPs in catalysis, the model reduction reaction of 4-nitrothiophenol (4-NTP) by $NaBH_4$ was chosen.[52, 53] This reaction can be easily followed by UV-Vis spectroscopy as 4-NTP absorbs strongly at 410 nm while the formed 4-aminothiophenol (4-ATP) presents an absorption band at 270 nm (Fig. 10). In the absence of metallic NPs, the reduction reaction requires more than 2 hours to be completed while in the presence of the synthesised Ag NPs the 4-NTP signal disappears in less than 15 min (Fig.10). This demonstrates the catalytic activity of the clusters stabilised by calixarenes. Even if the NPs are surrounded by calix[8]arenes grafted to their surface by sulphur atoms, the metallic sites are still accessible and the NPs keep some catalytic activity. It is to be noted that if 4-nitrophenol is used instead of 4-NTP, no reduction occurs, indicating that adsorption of the molecule on the NP surface is important as it may ease the NP to substrate electron transfer.

Conclusions

In summary, *p*-octa(hydroxy)-octa(mercapto) calix[8]arenes are able to stabilise small spherical and very homogeneous in size metallic NPs due to confinement, macrocyclic and cooperative effects. If the precursor salt has little influence on the produced NP size, the ratio metal/calix is an important parameter. Calix[8]arenes also allow the radiolytic formation of alloyed bimetallic NPs. So, these calix[8]arenes are very efficient in stabilising small and homogeneous NPs. The structure of the calix[8]arenes and its anchoring on the NP surface let some accessibility to the surface of the NPs, what is very important for applications in catalysis. Hence, calix[8]arene-stabilised NPs of different metals can find applications in catalysis or electrocatalysis. In addition, the possibility to synthesise different calix[8]arene-derivatives by modifying the functionalised groups on the upper rim offers many potential applications.

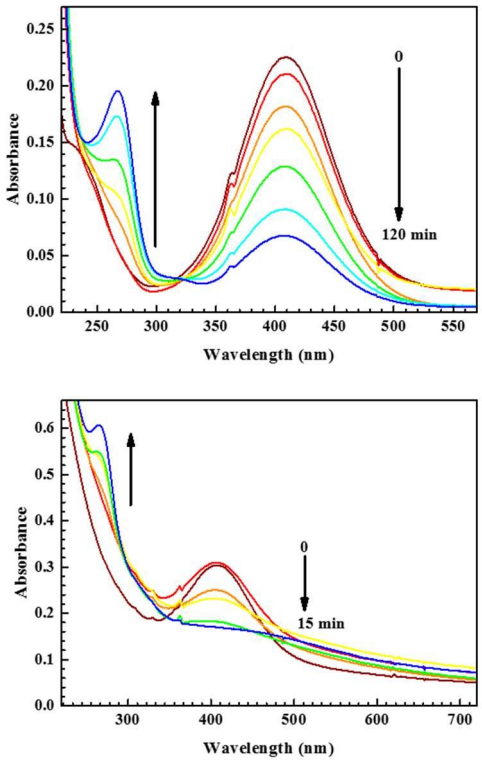

Fig. 10 UV-visible absorption spectra showing the reduction reaction of 4-NTP (4.4×10^{-5} M by $NaBH_4$ (0.044 M) in aqueous solutions **(top)** in the absence and **(bottom)** in the presence of Ag NPs ($[Ag^0] = 9.7 \times 10^{-6}$ M); the light scattering observed on the spectra (right) is due to a low solubility of the calix[8]arene-stabilised NPs in water; optical path = 1 cm.

Conflicts of interest

There are no conflicts to declare.

Acknowledgements

The authors acknowledge the France-Mexico ECOS Nord program M11P02 for financial support. They thank H. Silva (IPICYT, San Luis Potosi, Mexico) for TEM measurements. XPS spectra were obtained by Dr. M. Bravo Sanchez at the National Laboratory Research in Nanoscience and Nanotechnology (LINAN) at IPICYT (San Luis Potosi, Mexico). HAADF-STEM and STEM-EDX study were carried out within the MATMECA consortium, supported by the ANR-10-EQPX-37 contract and has benefited from the facilities of the Laboratory MSSMat (UMR CNRS 8579), CentraleSupelec, France. The authors are grateful for the technical assistance of F. Fossard (LEM, CNRS-ONERA, France).They also thank Inside Vision Lab (http://www.invilab.com/) and Ekaterina Shilova for design assistance.

Notes and references

§ It must be noted that irradiation of solutions containing metallic salts and calix[8]arenes **5** either just after mixing (i.e. exhibiting light scattering pattern) or after overnight stirring (i.e. with weak scattering pattern) give similar results for the NPs formation.

1. M. El Sayed, *Acc. Chem. Res*, 2001, **34**, 257-264.
2. K. L. Kelly, E. Coronado, L. L. Zhao and G. C. Schatz, *J. Phys. Chem. B*, 2003, **107**, 668-677.
3. C. C. Baker, A. Pradhan and S. I. Shah, *Encyl. Nanosci. Nanotechnol.*, 2004, **5**, 449-474.
4. S. P. Gubin, Y. A. Koksharov, G. B. Khomutov and G. Y. Yurkov, *Russ. Chem. Rev.*, 2005, **74**, 489-520.
5. E. Roduner, *Chem. Soc. Rev.*, 2006, **35**, 583-592.
6. M.-C. Daniel and D. Astruc, *Chem. Rev.*, 2004, **104**, 293-346.
7. D. Astruc, F. Lu and J. R. Aranraes, *Angew. Chem. Int. Ed.*, 2005, **44**, 7852-7872.
8. R. Jin, *Nanotechnol. Rev.*, 2012, **1**, 31-56.
9. H. Hu, H. Hu, X. Wang, D. Miao and Y. Lu, *J. Mater. Chem. A*, 2015, **3**, 11157-11182.
10. S. Cao, F. F. Tao, Y. Tang, Y. Li and J. Yu, *Chem. Soc. Rev.*, 2016, **45**, 4747-4765.
11. V. E. Ferry, L. A. Sweatlock, D. Pacifici and H. A. Atwater, *Nano Lett.*, 2008, **8**, 4391-4397.
12. P. Zijlstra, J. W. Chon and M. Gu, *Nature*, 2009, **459**, 410-413.
13. M. Arruebo, R. Fernandez-Pacheco, M. R. Ibarra and J. Santamaria, *Nano today*, 2007, **2**, 22-32.
14. Y.-W. Jun, J.-W. Seo and J. Cheon, *Acc. Chem. Res.*, 2008, **41**, 179-189.
15. B. Sepulveda, P. C. Angelomé, L. M. Lechuga and L. M. Liz-Marzan, *Nano today*, 2009, **4**, 244-251.
16. R. Guo, L. Zhang, H. Qian, R. Li, X. Jiang and B. Liu, *Langmuir*, 2010, **26**, 5428-5434.
17. E. Boisselier and D. Astruc, *Chem. Soc. Rev.*, 2009, **38**, 1759-1782.
18. S. K. Ghosh and T. Pal, *Chem. Rev.*, 2007, **107**, 4797-4862.
19. M. Rycenga, C. M. Cobley, J. Zeng, W. Li, C. H. Moran, Q. Zhang, D. Qin and Y. Xia, *Chem. Rev.*, 2011, **111**, 3669-3712.
20. M. A. Garcia, *J. Phys. D: Appl. Phys.*, 2011, **44**, 283001.
21. S. Schlücker, *Angew. Chem. Int. Ed.*, 2014, **53**, 4756-4795.
22. M. Li, S. K. Cushing and N. Wu, *Analyst*, 2015, **140**, 386-406.
23. Z.-J. Jiang, C.-Y. Liu and L.-W. Sun, *J. Phys. Chem. B*, 2005, **109**, 1730-1735.
24. M. Haruta and M. Daté, *Appl. Catal. A: gen.*, 2001, **222**, 427-437.
25. J. S. Kim, E. Kuk, K. N. Yu, J.-H. Kim, S. J. Park, H. J. Lee, S. H. Kim, Y. K. Park, Y. H. Park, C.-Y. Hwang, Y.-K. Kim, Y.-S. Lee, D. H. Jeong and M.-H. Cho, *Nanomedecine: Nanotech., Biol. Med.*, 2007, **3**, 95-101.
26. L. S. Nair and C. T. Laurencin, *J. Biomed. Nanotechnol.*, 2007, **3**, 301-316.
27. S. Her, D. A. Jaffray and C. Allen, *Adv. Drug Deliv. Rev.*, 2017, **109**, 84-101.
28. V. K. Sharma, R. A. Yngard and Y. Lin, *Adv. Colloid. Interfac. Sci.*, 2009, **145**, 83-96.
29. J. Liu, W. Ong and A. E. Kaifer, *Langmuir*, 2002, **18**, 5981-5983.
30. V. I. Bhoi, S. Kumar and C. N. Murthy, *New. J. Chem.*, 2016, **40**, 1396-1402.
31. T. Premkumar, Y.-S. Lee and K. E. Geckeler, *Chem. Eur. J.*, 2010, **16**, 11563-11566.
32. X. Lu and E. Masson, *Langmuir*, 2011, **27**, 3051-3058.
33. A. Wei, *Chem. Comm.*, 2006, 1581-1591.
34. A. R. Kongor, V. A. Mehta, K. M. Modi, M. K. Panchal, S. A. Dey, U. S. Panchal and V. K. Jain, *Top Curr. Chem.* , 2016, **374**, 28.
35. R. Perrin, R. Lamartine and M. Perrin, *Pure & Appl. Chem.*, 1993, **65**, 1549-1559.
36. G. McMahon, S. O'Malley and K. Nolan, *ARKIVOC*, 2003, **(vii)**, 23-31.
37. J.-M. Ha, A. Solovyov and A. Katz, *Langmuir*, 2009, **25**, 10548-10553.
38. N. de Silva, J.-M. Ha, A. Solovyov, M. M. Nigra, I. Ogino, S. W. Yeh, K. A. Durkin and A. Katz, *Nature Chem.*, 2010, **2**, 1062-1068.
39. J.-M. Ha, A. Solovyov and A. Katz, *J. Phys. Chem. C*, 2010, **114**, 16060-16070.
40. G. J. Hutchings, *Nature Chem.*, 2010, **2**, 1005-1006.
41. V. Huc and K. Pelzer, *J. Colloid Interface Sci.*, 2008, **318**, 1-4.
42. K. J. Hartlieb, M. Saunders and C. L. Raston, *Chem. Comm.*, 2009, 3074-3076.
43. K. J. Hartlieb, A. D. Martin, M. Saunders and C. L. Raston, *New. J. Chem.*, 2010, **34**, 1834-1837.
44. S. Gao, D. Yuan, J. Lu and R. Cao, *J. Colloid Interf. Sci.*, 2010, **341**, 320-325.
45. J. Belloni, M. Mostafavi, H. Remita, J.-L. Marignier and M.-O. Delcourt, *New. J. Chem.*, 1998, **22**, 1239-1255.
46. H. Remita, I. Lampre, M. Mostafavi, E. Balanzat and S. Bouffard, *Radiat. Phys. Chem.*, 2005, **72**, 575-586.
47. W. Abidi and H. Remita, *Recent Patent on Engineering*, 2010, **4**, 170-188.
48. A. Abedini, A. A. A. Bakar, F. Larki, P. S. Menon, M. S. Islam and S. Shaari, *Nanoscale Res. Lett.*, 2016, **11**, 287.
49. I. P. Bell and M. A. J. Rodgers, *J. Chem. Soc. Faraday Trans. 1*, 1977, **73**, 315-326.
50. C. Ferradini and J.-P. Jay-Gerin, *Radiat. Phys. Chem.*, 1996, **48**, 473-480.
51. C. Ferradini and J.-P. Jay-Gerin, *Can. J. Chem.*, 1999, **77**, 1542-1575.
52. T. Aditya, A. Pal and T. Pal, *Chem. Comm.*, 2015, **51**, 9410-9431.
53. P. Zhao, X. Feng, D. Huang, G. Yang and D. Astruc, *Coord. Chem. Rev.*, 2015, **287**, 114-136.
54. J. J. J. Myron and G. R. Freeman, *Can. J. Chem.*, 1965, **43**, 381-394.

55. J. C. Russell and G. R. Freeman, *J. Phys. Chem.*, 1967, **71**, 755-762.
56. J. Belloni and J.-L. Marignier, *Radiat. Phys. Chem.*, 1989, **34**, 157-171.
57. M. Mostafavi, G. R. Dey, L. François and J. Belloni, *J. Phys. Chem. A*, 2002, **106**, 10184-10194.
58. B. Soroushian, I. Lampre, J. Belloni and M. Mostafavi, *Radiat. Phys. Chem.*, 2005, **72**, 111-118.
59. H. A. Schwarz and R. W. Dodson, *J. Phys. Chem.*, 1989, **93**, 409-414.
60. E. Gachard, H. Remita, J. Khatouri, B. Keita, L. Nadjo and J. Belloni, *New. J. Chem.*, 1998, **22**, 1257-1265.
61. A. Henglein, *Ber. Bunsenges Phys. Chem.*, 1977, **81**, 556-561.
62. S. Rémita, M. Mostafavi and M.-O. Delcourt, *J. Phys. Chem.*, 1996, **100**, 10187-10193.
63. I. Texier, S. Rémita, P. Archirel and M. Mostafavi, *J. Phys. Chem.*, 1996, **100**, 12472-12476.
64. M. Mostafavi and J. Belloni, *Recent Res. Devel. in Physical Chem.*, 1997, **1**, 459-474.
65. I. Lampre, P. Pernot and M. Mostafavi, *J. Phys. Chem. B*, 2000, **104**, 6233-6239.
66. A. Henglein, *Chem. Rev.*, 1989, **89**, 1861-1873.
67. J. Belloni, *Catal. today*, 2006, **113**, 141-156.
68. R. Tausch-Treml, A. Henglein and J. Lilie, *Ber. Bunsenges Phys. Chem.*, 1978, **82**, 1335-1343.
69. G. R. Dey, A. K. El Omar, J. A. Jacob, M. Mostafavi and J. Belloni, *J. Phys. Chem. A*, 2011, **115**, 383-391.
70. M. Treguer, C. de Cointet, H. Remita, J. Khatouri, M. Mostafavi, J. Amblard and J. Belloni, *J. Phys. Chem. B*, 1998, **102**, 4310-4321.
71. A. Casnati, R. Ferdani, A. Pochini and R. Ungaro, *J. Org. Chem.*, 1997, **62**, 6236-6239.
72. W. Sliwa and M. Deska, *ARKIVOC*, 2008, **(i)**, 87-127.
73. Y. Zhou, C. Liu, H. Xu, H. Yu, Q. Lu and L. Wang, *Spectrochim. Acta A*, 2007, **66**, 919-923.
74. L. J. Hubble, R. A. Boulos and C. L. Raston, *New. J. Chem.*, 2012, **36**, 1070-1079.
75. J. Zhan, L. Wen, F. Miao, D. Tian, X. Zhu and H. Li, *New. J. Chem.*, 2012, **36**, 656-661.
76. N. V. Rathod, K. Joshi, A. S. Jadhav, V. S. Kalyani, K. Selvaraj and D. D. Malkhede, *Polyhedron*, 2017, **137**, 207-2016.
77. F. Baletto and R. Ferrando, *Rev. Mod. Phys.*, 2005, **77**, 371-423.
78. A. M. Angulo and N. C., *J. Phys. Chem. A*, 2008, **112**, 5834-5838.
79. M. Yamada, H. Hagiwara, H. Torigoe, N. Matsumoto, M. Kojima, F. Dahan, J.-P. Tuchagues, N. Re and S. Iijima, *Chem. Eur. J.*, 2006, **12**, 4536-4549.
80. J. H. Kim, B. R. Min, J. Won and Y. S. Kang, *Macromol. Res.*, 2006, **14**, 199-204.
81. M. Sankar, N. Dimitratos, P. J. Miedziak, P. P. Wells, C. J. Kiely and G. J. Hutchings, *Chem. Soc. Rev.*, 2012, **41**, 8099-8139.
82. K. D. Gilroy, A. Ruditskiy, H.-C. Peng, D. Qin and Y. Xia, *Chem. Rev.*, 2016, **116**, 10414-10472.
83. M. S. Holden, K. E. Nick, M. Hall, J. R. Milligan, Q. Chen and C. C. Perry, *RSC Adv.*, 2014, **4**, 52279-52288.
84. J. D. Padmos, M. Langman, K. MacDonald, P. Comeau, Z. Yang, M. Filiaggi and P. Zhang, *J. Phys. Chem. C*, 2015, **119**, 7472-7482.
85. G. Guisbiers, R. Mendoza-Cruz, L. Bazán-Díaz, J. J. Velázquez-Salazar, R. Mendoza-Perez, J. A. Robledo-Torres, J.-L. Rodriguez-Lopez, J. M. Montejano-Carrizales, R. L. Whetten and M. J. Yacamán, *ACS Nano*, 2016, **10**, 188-198.
86. N. S. K. Gowthaman, B. Sinduja and S. A. John, *RSC Adv.*, 2016, **6**, 63433-63444.
87. A. McNeillie, D. H. Brown, W. E. Smith, M. Gibson and L. Watson, *J. Chem. Soc. Dalton Trans.*, 1980, 767-770.
88. G. Xue, M. Ma, J. Zhang, Y. Lu and K. Carron, *J. Colloid Interf. Sci.*, 1992, **150**, 1-6.
89. A. J. Leavitt and T. P. Beebe, *Surf. Sci.* , 1994, **314**, 23-33.
90. H. Peisert, T. Chassé, P. Streubel, A. Meisel and R. Szargan, *J. Electron Spectrosc. Relat. Phenom.*, 1994, **68**, 321-328.
91. L. Carlini, C. Fasolato, P. Postorino, I. Fratoddi, I. Venditti, G. Testa and C. Battocchio, *Colloids Surf. A*, 2017, **532**, 183-188.
92. M. Romand, M. Roubin and J. P. Deloume, *J. Electron Spectrosc. Relat. Phenom.*, 1978, **13**, 229-242.
93. B. V. R. Chowdari, K. F. Mok, J. M. Xie and R. Gopalakrishnan, *J. Non-Cryst. Solids*, 1993, **160**, 73-81.
94. M. P. Casaletto, A. Longo, A. Martorana, A. Prestianni and A. M. Venezia, *Surf. Interface Anal.*, 2006, **38**, 215-218.
95. E. Bedford, V. Humblot, C. Méthivier, C.-M. Pradier, F. Gu, F. Tielens and S. Boujday, *Chem. Eur. J.*, 2015, **21**, 14555-14561.

View Article Online
DOI: 10.1039/C8NJ02451K

View Article Online
DOI: 10.1039/C8NJ02451K

Table of contents

We report a facile approach to synthesise small Au-Ag alloyed nanoparticles using a new cali[8]arene derivative as stabiliser.